

Microstructure and mechanical property of Cu/In–45Cu/Ni solder joints formed by transient liquid phase bonding

Li Yang^{1,2,a)}, Shiyuan Zhou^{3,b)}, Yaocheng Zhang², Yifeng Xiong², Wei Jiang², Sai Shen²

¹School of Mechanical Engineering, Guilin University of Aerospace Technology, Guilin 541004, P.R. China

²School of Automotive Engineering, Changshu Institute of Technology, Jiangsu 215500, P.R. China

³School of Mechanical and Electrical Engineering, Soochow University, Jiangsu 215000, P.R. China

^{a)}Address all correspondence to these authors. e-mail: linlideyu@126.com

^{b)}e-mail: 963905640@qq.com

Received: 22 April 2020; accepted: 9 July 2020

In this paper, the microstructure and the shear property of Cu/In–45Cu/Ni solder joints by transient liquid phase were studied, and the intermetallic compounds (IMCs) growth mechanism was investigated. The results showed that the IMCs volume ratio of solder joints was increased firstly and then decreased with increasing bonding time, and the IMCs volume ratio reached its maximum value of 95.8% at 60 min. The Cu interfacial IMC of the solder joint with dense microstructure was Cu₂In phase at 60 min, and the Ni interfacial IMC was Ni₃In₇. The maximum shear strength of solder joints was obtained at 60 min, which is 15.21 MPa. The shear fracture appeared honeycomb structure, and the fracture occurred at the phase interface of Ni₃In₇/Cu₁₁In₉. The thickness of the interfacial IMCs and the white IMCs around the Cu particles (Cu@IMC) was increased continuously with increasing bonding time, and thus, the interconnection of Cu–Ni substrates was realized ultimately.

Introduction

The wide band gap semiconductor materials are widely used in aerospace, petrochemical, rail transportation, clear energy, and many other fields due to its excellent electronic, physical, chemical, and mechanical properties [1]. The third-generation wide band gap semiconductor materials represented by SiC and GaN have become the most important semiconductor materials for manufacturing high-frequency power electronic devices, short-wavelength optoelectronic devices, and high-temperature and radiation-resistant devices, which can be used up to 300 °C [2, 3]. However, the electronic interconnection materials tend to fracture in high-temperature environment, and the reliability of interconnect solder joints in electronic products has become a key issue affecting system reliability [4, 5]. Therefore, the development of packaging technologies and connection materials used at high temperature is of great significance to the electronic packaging industry [6]. In recent years, transient liquid phase (TLP) bonding as a new type of packaging technology has attracted more and more attention due to its simple process and low cost [7, 8, 9].

As a superior substrate material, Cu is widely used in the electronic packaging field due to its excellent electrical conductivity, good thermal conductivity, and strong corrosion

resistance. The fast reaction rate between Cu and solders results in the rapid growth of intermetallic compounds (IMCs) at the interface, and then, the reliability of solder joints is degraded dramatically [10]. Ni is frequently used as the diffusion barrier in under bump metallurgy on the chip side to inhibit the rapid formation of interfacial IMCs during soldering [11, 12]. Therefore, the connection of the Cu/Ni sandwich structure would be encountered in electronic devices, and the reactions of Cu/Ni joints during soldering crucially determine the reliability of devices.

Lots of researches were carried out on the microstructure and mechanical properties of Cu/Ni TLP joints by using Sn-based solders, such as pure Sn [13, 14, 15], Sn–0.7Cu [16], Sn–Ag [17], and Sn–9Zn [18]. Dong [13] found that the IMCs transformed from (Cu, Ni)₆Sn₅ into Cu₃Sn on the Cu interface from 30 to 120 min. The shear strength of the Cu/Sn/Ni solder joint was 49.8 ± 0.3 MPa at 120 min, and the shear fracture was inclined to occur in the area of (Cu, Ni)₆Sn₅ grains with the coarse rounded shape. Mo [14] pointed out that the IMCs in the Cu/Sn/Ni solder joints were (Cu, Ni)₃Sn on the Cu substrate and (Cu, Ni)₆Sn₅ IMCs on the Ni substrate at 240 °C, and the (Cu, Ni)₆Sn₅ was converted to (Cu, Ni)₃Sn with the bonding temperature was increased

to 290 °C. The fracture mode of the solder joint at 290 °C was the brittle fracture mode with intergranular and transgranular fracture surfaces. Zhong [15] proved that the continuous $(\text{Cu}_{0.95}, \text{Ni}_{0.05})_6\text{Sn}_5$ IMC formed on the Cu interface, while $(\text{Cu}_{0.76}, \text{Ni}_{0.24})_6\text{Sn}_5$ IMC formed on the Ni interface. The interfacial IMCs at the cold end grew remarkably faster than that at the hot end under thermal migration, and the IMC growth rate on the Cu substrate was larger than that on the Ni substrate under the same conditions. Ji [16] showed that the IMCs in the Cu/Sn–0.7Cu/Ni solder joint consisted of $(\text{Cu}, \text{Ni})_6\text{Sn}_5$ and Cu_3Sn after ultrasonic-assisted die bonding of 10 s, and the shear strength was about 80.7 MPa. Huang [17] investigated the interfacial reactions of Ni/SnAg/Cu solder joints during TLP soldering. They found that the IMCs growth rate on the Ni side was larger than that on the Cu side in the Cu/Ni joint by 40 μm thick solder, while the growth reversed with the solder thickness was decreased below 20 μm. Zhao [18] found that the $(\text{Ni}, \text{Cu}, \text{Zn})_5\text{Zn}_{21}$ IMC was formed on the Ni interface at 250°C for 5 min, and the IMC on the Cu interface was Cu_5Zn_8 . The IMC was transformed to $(\text{Ni}, \text{Cu})_3(\text{Sn}, \text{Zn})_4$ on the Ni interface with the bonding time is increased to 240 min, and which of that on the Cu side were $\text{Cu}_6(\text{Sn}, \text{Zn})_5$ and $(\text{Cu}, \text{Ni})(\text{Zn}, \text{Sn})$.

In recent years, indium (In) solder has become one of the indispensable solders in the modern electronic packaging field due to its low melting point, good fatigue resistance and conductivity, and it is expected to become a solder to replace Sn solder [19]. The required bonding temperature of the solder joint by using In solder is lower than that of the solder joint by using Sn solder, and the high re-melting IMC phases are formed in the In/Cu solder joint [20].

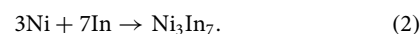
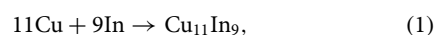
There was currently little research on the connection between Cu and Ni substrates by using In solder. Lin [21] investigated the interfacial reactions of Cu/In/Ni solder joints at 280°C. In solder was completely consumed in the solder joint after bonding of 1440 min, and the IMCs in the joint consisted of Ni_3In_7 and $\text{Cu}_{11}\text{In}_9$ phases. The $\text{Cu}_{11}\text{In}_9$ is divided into $\text{Cu}_{11}\text{In}_9$ (i) phase on the Cu interface and $\text{Cu}_{11}\text{In}_9$ (ii) phase with faceted rod-like morphology in the *in situ* reaction zone.

At present, the researches about the connection of the Cu/In–Cu/Ni composite solder joint were seldom reported. In the paper, the In–45Cu composite solder powders were prepared after adding about 45 wt% micron-sized Cu particles into the pure In solder powder, and then, the Cu/In–45Cu/Ni encapsulated solder joints were obtained by TLP bonding. The microstructure and the fracture morphologies of Cu/In–45Cu/Ni solder joints were observed. The shear strength of Cu/In–45Cu/Ni solder joints was tested. The IMCs growth mechanism of the Cu/In–45Cu/Ni solder joints was investigated.

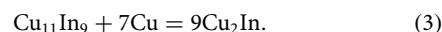
Results and Discussion

Microstructure

Figure 1 shows the microstructure of Cu/In–45Cu/Ni solder joints at different bonding times. As shown in Fig. 1, the Cu/In–45Cu/Ni solder joints can be divided into three parts: interfacial diffusion reaction zone I on the Cu substrate, *in situ* reaction zone II and interfacial diffusion reaction zone III on the Ni substrate, and Cu particles basically no longer existed in the solder joint after bonding for 15–120 min. The numerous voids and residual In phase exist in the solder joint at 15 min [Fig. 1(a)]. Energy-dispersive spectroscopy (EDS) results show that the interfacial IMC at the Cu substrate is $\text{Cu}_{11}\text{In}_9$, the interfacial IMC at the Ni substrate is Ni_3In_7 , and the IMC in the *in situ* reaction zone is $\text{Cu}_{11}\text{In}_9$. The same results are obtained by Lin [21], and the chemical reaction formulas are given as follows [22, 23]:



The voids and the residual In phase in the solder joints are decreased firstly and then increased with increasing bonding time. However, the IMCs in the *in situ* reaction zone are increased firstly and then decreased. As shown in Fig. 1(c), the Cu/In–45Cu/Ni solder joint is well connected when the bonding time is up to 60 min. The molten In particles continuously access the gap in the solder joint and react adequately with Cu particles to form In–Cu compounds after long bonding time. EDS results show that the interfacial IMC at the Cu substrate is transformed from $\text{Cu}_{11}\text{In}_9$ phase into Cu_2In phase, and granule-like Cu_2In phase appears in the *in situ* reaction zone [20]:



However, the continuous voids appear on the Ni side of the Cu/In–45Cu/Ni solder joint at 120 min. The Kirkendall effect is the reason of the voids formation [24, 25, 26]. More Cu_2In phase is produced with longer bonding time, and the Kirkendall effect became more serious, as shown in Fig. 1(d). Tian [20] also finds that the Kirkendall effect is significant during the microstructure evolution of Cu/In/Cu joints, and Kirkendall voids occur along the Cu interface after bonding for 40 min. Other studies report this phenomenon in Cu/Sn/Cu systems, and the voids are usually located along the Cu/ Cu_3Sn interface [27, 28].

The average thickness of interfacial IMC in the diffusion reaction zone I and III is measured by ImageJ software, and its change trend can be clearly expressed. As shown in Fig. 2,

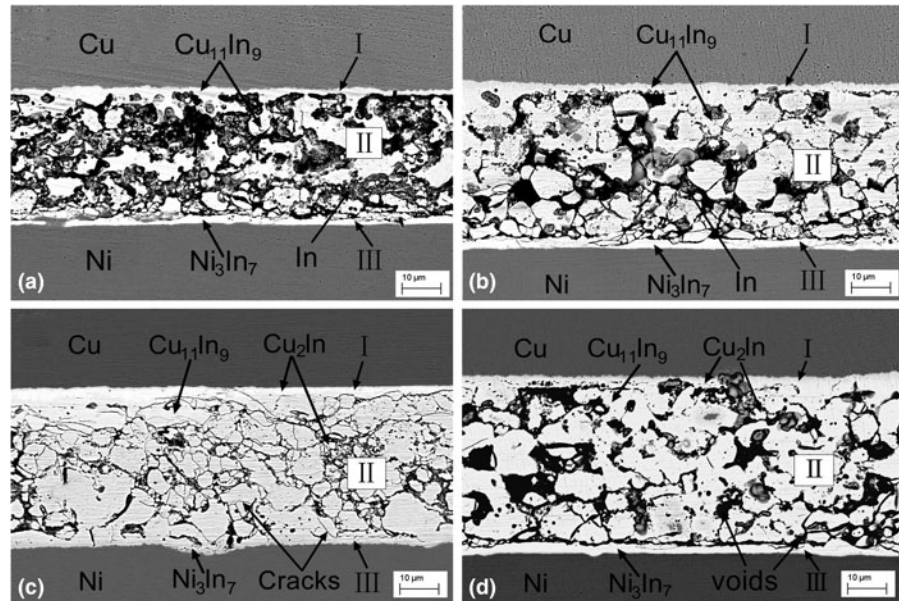


Figure 1: Microstructure of Cu/In-45Cu/Ni solder joints at different bonding times: (a) 15 min, (b) 30 min, (c) 60 min, and (d) 120 min.

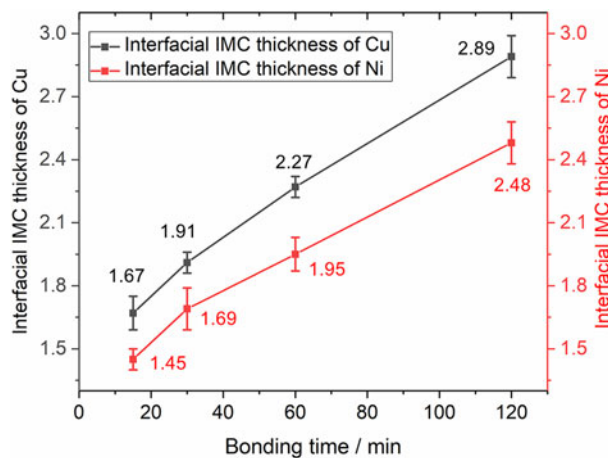


Figure 2: Relationship between interfacial IMC thickness and bonding time.

the interfacial IMC thickness of the Cu substrate and Ni substrate is about 1.67 and 1.45 μm at 15 min, respectively, and they are both increased with increasing bonding time. The IMC thickness in the diffusion reaction zone I of the Cu substrate interface is larger than IMC thickness in the diffusion reaction zone III of the Ni substrate interface at the same bonding time. It indicates that the diffusion rate of Cu atoms is greater than that of Ni atoms under the same bonding conditions. The EDS results of the Cu/In-45Cu/Ni solder joint at 120 min are shown in Fig. 3. As shown in Fig. 3(a), the number of Ni atoms is negligible in the *in situ* reaction zone. The same result is obtained by the EDS element mapping [Fig. 3(b)]. The similar results are obtained by Chen [29] and Rizvi [30]. Chen suggests that the diffusivity of Cu atoms in Sn solder is two orders of magnitude higher than that of Ni atoms, causing

that Cu atoms would easily diffuse across the bulk solder than Ni atoms and influence the interfacial reactions. Rizvi considers that Cu atoms diffuse into the Sn-2.8Ag-0.5Cu-1.0Bi solder through the IMCs much faster than that of Ni atoms.

The IMCs volume ratio of Cu/In-45Cu/Ni solder joints at different bonding times is shown in Fig. 4. As shown in Fig. 4, the IMCs volume ratio is increased firstly and then decreased with increasing bonding time, and the maximum IMCs volume ratio is obtained at 60 min, which is 95.8%. Combining with Fig. 1(c), a small amount of cracks occur in the *in situ* reaction zone of the solder joint at 60 min, and it is caused by the volume contraction after the IMCs transformation.

The crystal structure is obtained by materials studio software. $\text{Cu}_{11}\text{In}_9$ phase is C2/m oblique crystal structure [31], and Cu_2In phase is P63/mmc hexagonal structure. The lattice constants of $\text{Cu}_{11}\text{In}_9$ phase are $a = 13.027$ nm, $b = 4.406$ nm, $c = 7.460$ nm, and $\beta = 54.22^\circ$. The lattice constants of Cu_2In phase are $a = b = 4.471$ nm and $c = 5.384$ nm. The density of $\text{Cu}_{11}\text{In}_9$ and Cu_2In is given as follows:

$$\rho_{\text{Cu}_{11}\text{In}_9} = \frac{11M_{\text{Cu}} + 9M_{\text{In}}}{N_A abc \sin \beta} = 8.28 \text{ g/cm}^3, \quad (4)$$

$$\rho_{\text{Cu}_2\text{In}} = \frac{4M_{\text{Cu}} + 2M_{\text{In}}}{N_A abc} = 7.46 \text{ g/cm}^3, \quad (5)$$

where $\rho_{\text{Cu}_{11}\text{In}_9}$ is the density of $\text{Cu}_{11}\text{In}_9$ phase; M_{Cu} , M_{In} are the molar mass of Cu and In, respectively; N_A is the Avogadro constant. The density of Cu and In is 8.92 and 7.31 g/cm³, respectively, and then, the volume change of 11 mol Cu and 9 mol In after reacting and completely transforming to 1 mol

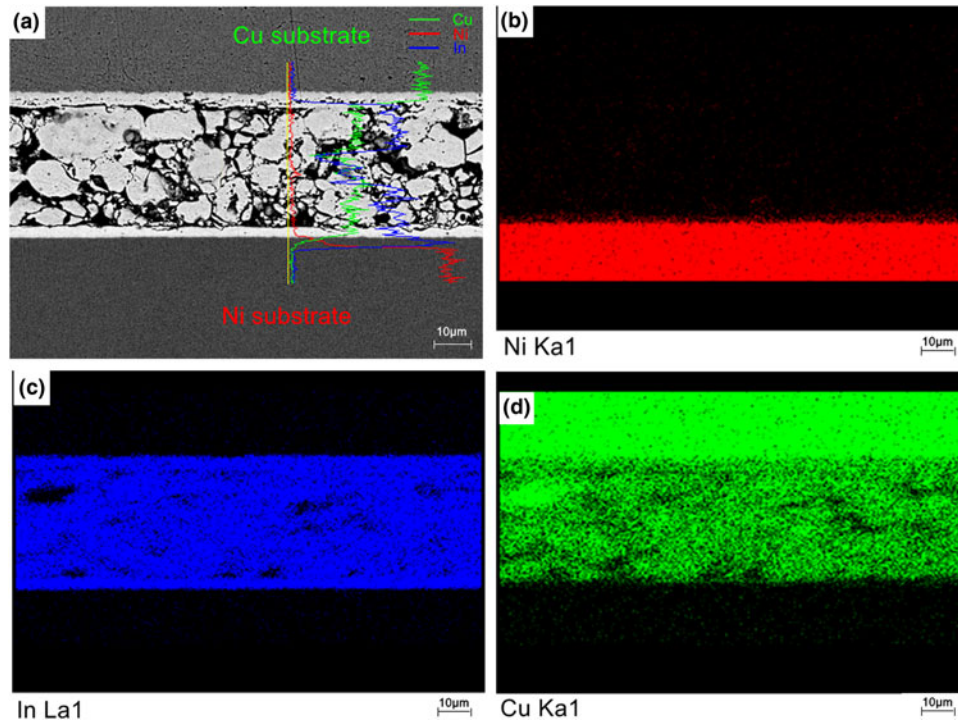


Figure 3: EDS results of the Cu/In-45Cu/Ni solder joint at 120 min (a) line-scanning and (b–d) Ni, In, and Cu elemental mapping images.

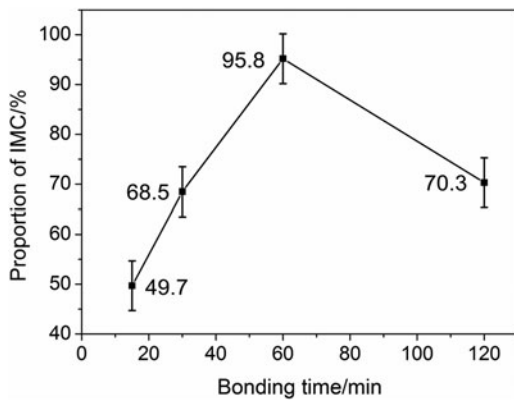


Figure 4: IMCs volume ratio of Cu/In-45Cu/Ni solder joints at different bonding times.

$\text{Cu}_{11}\text{In}_9$ can be expressed as follows:

$$\Delta V = \frac{11M_{\text{Cu}} + 9M_{\text{In}}}{\rho_{\text{Cu}_{11}\text{In}_9}} - \frac{11M_{\text{Cu}}}{\rho_{\text{Cu}}} - \frac{9M_{\text{In}}}{\rho_{\text{In}}} = -10.5 \text{ cm}^3. \quad (6)$$

Then, the volume shrinkage rate is obtained:

$$K = \frac{\Delta V}{11V_{\text{In}} + 9V_{\text{Cu}}} = \frac{-10.5}{78.3 + 141.3} = -4.8\%. \quad (7)$$

Similarly, the volume change is 32.75 cm^3 , and the volume expansion rate is 12.65% after 1 mol $\text{Cu}_{11}\text{In}_9$ and 7 mol Cu being converted into 9 mol Cu_2In . The solder joint is composed of a large amount of $\text{Cu}_{11}\text{In}_9$ phase and a small amount

of Cu_2In phase at 60 min, and thus, the volume change is mainly manifested in volume shrinkage, which inevitably leads to a small amount of cracks in the *in situ* reaction zone. The volume shrinkage also appears in the Cu/Sn system. Sun [32] and Pan [33] find that the volume shrinkage is about 4.38 and 4.4% after the reaction of Cu_6Sn_5 transforms to Cu_3Sn , respectively.

The IMCs volume ratio is decreased to 70% when the bonding time is increased to 120 min, combining with Fig. 1 (d), the voids and cracks exist in the solder joint at 120 min. In summary, the Cu/In-45Cu/Ni solder joint with dense microstructure can be obtained by a bonding temperature of 260 °C, a bonding pressure of 5 MPa, and a bonding time of 60 min.

Shear property

Figure 5 shows the effect of bonding time on the shear strength of Cu/In-45Cu/Ni solder joints. As shown in Fig. 5, the shear strength is increased firstly and then decreased with increasing bonding time. The shear strength of the solder joint is 12.53 MPa at 15 min, and the maximum value of 15.21 MPa is obtained at 60 min. Combining with Fig. 1, the dense microstructure of the solder joint is obtained at 60 min and IMCs volume ratio reaches the maximum value. Therefore, the joint is well connected, which effectively improves the bonding strength of the solder joint. Furthermore, the Cu_2In phase is

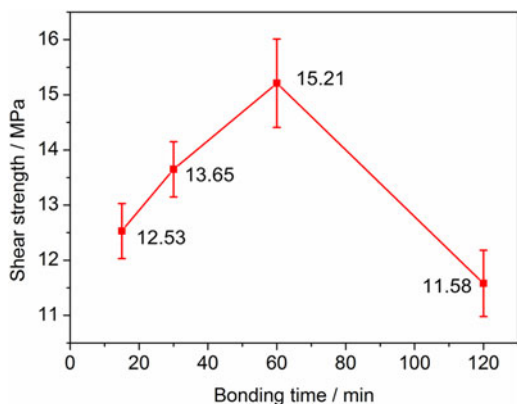


Figure 5: Shear strength of Cu/In-45Cu/Ni solder joints at different bonding times.

increased in the solder joint with the bonding time is increased to 60 min, and the Cu_2In phase has better shear strength compared with $\text{Cu}_{11}\text{In}_9$ phase. The tensile strength of the solder joint consisting entirely of $\text{Cu}_{11}\text{In}_9$ IMC is 5.08 MPa, and that of the solder joint consisting entirely of Cu_2In IMC is 13.65 MPa. In addition, the fractures of solder joints both occur in the IMCs phases. Therefore, the tensile strength of Cu_2In phase is greater than that of $\text{Cu}_{11}\text{In}_9$ phase [20]. According to the Cu-In phase diagram, the melting points of $\text{Cu}_{11}\text{In}_9$ and Cu_2In phases are 307 and 631 °C. As the melting point of Cu_2In was much higher than that of $\text{Cu}_{11}\text{In}_9$, the Cu_2In phase is more stable thermally and more suitable to improve the mechanical properties of Cu/In-45/Ni interconnections [20]. The shear strength of the solder joint is decreased to the minimum value of 11.58 MPa when the bonding time is 120 min. The continuous voids occur at the interface of substrate/IMCs [Fig. 1(d)], which greatly reduces the bond strength of the solder joint, resulting that the shear strength of the solder joint is significantly decreased.

In summary, the superior shear strength of the Cu/In-45Cu/Ni solder joint is obtained after bonding for 60 min, which is 15.21 MPa. Similar results are obtained by other researches. Tian [20] finds that the maximum shear strength of the Cu/In/Cu solder joint is 13.65 MPa, and the maximum shear strength 15.21 MPa obtained by our experiment is 11.43% greater than this value. Lee [34] considers the maximum shear strength of the Cu/In/Cu solder joint is 16.8 MPa.

Figure 6 shows the fracture morphologies of Cu/In-45Cu/Ni solder joints at different bonding times. The fracture shows a large amount of In particles and a small amount of $\text{Cu}_{11}\text{In}_9$ IMC at 15 min [Fig. 6(a)]. Combining with Fig. 1(a), the Cu/In-45Cu/Ni solder joint consists of a large amount of residual In particles and $\text{Cu}_{11}\text{In}_9$ phase the *in situ* reaction zone. It is prone to fracture during the shearing process due to the bad connection of the solder joint. The amount of In particles is decreased in the fracture with increasing bonding time, and

the proportion of IMCs is increased. At 60 min, the fracture surface of the solder joint shows the IMCs morphology. EDS results show that IMCs are Ni_3In_7 and $\text{Cu}_{11}\text{In}_9$ phases, and the intergranular brittle fracture occurs at the interface of $\text{Cu}_{11}\text{In}_9/\text{Ni}_3\text{In}_7$ near the Ni substrate. The magnification of region A in Fig. 6(c) is shown in Fig. 6(d), and the fracture surface shows a uniform honeycomb-like structure.

The shear fracture process of the Cu/In-45Cu/Ni solder joint at 60 min is shown in Fig. 7, and the solder joint fractures at the interface of cylindrical $\text{Cu}_{11}\text{In}_9$ and Ni_3In_7 phases under the shear stress. After the separation of cylindrical $\text{Cu}_{11}\text{In}_9$ IMC and Ni_3In_7 IMC on the Ni substrate, a honeycomb-like structure appears in the fracture of the Ni substrate. The cracks at the phase boundaries of IMCs have a significant influence on the fracture mode of the solder joint [35, 36, 37]. According to the principle of minimum energy, the cracks propagation direction follows the path of least resistance, and thus, it is determined by the relationship between the grain boundaries strength and the strength of grain interior [38, 39]. The intra-grain strength of IMCs gains is greater than the grain boundaries strength; therefore, the cracks initiate firstly in the voids and propagate along the grains boundaries when the solder joint is subjected to a shear deformation, resulting in the fracture of the solder joint [40, 41]. A number of voids exist at the interface of $\text{Cu}_{11}\text{In}_9$ and Ni_3In_7 phases boundaries, and the strength of the phase interior is greater than that of the phase boundaries. Therefore, the Cu/In-45Cu/Ni solder joint at 60 min is liable to fracture at the interface of $\text{Cu}_{11}\text{In}_9/\text{Ni}_3\text{In}_7$ phases on the Ni substrate under the shear stress.

The fracture surface shows granular IMCs morphology when the bonding time is increased to 120 min [Fig. 6(d)], and the IMCs are divided into cylindrical $\text{Cu}_{11}\text{In}_9$ phase and small granular Cu_2In phase from EDS results. After long-time bonding, the cracks along the interface of $\text{Cu}_{11}\text{In}_9$ and Cu_2In phases are increased due to the volume shrinkage, and thus, the shear fracture is likely to occur $\text{Cu}_{11}\text{In}_9/\text{Cu}_2\text{In}$ interface.

IMCs growth mechanism

The microstructure of Cu/In-45Cu/Ni solder joints at 0.5–20 min is shown in Fig. 8. As shown in Fig. 8, the *in situ* reaction zone of the solder joints with the sandwich structure consists of In-rich phase, Cu particles, and Cu@IMC, and the thin interfacial IMCs exist at Cu and Ni substrates. EDS results show that the Cu@IMC in the *in situ* reaction zone and the interfacial IMC on the Cu substrate both are $\text{Cu}_{11}\text{In}_9$, and the interfacial IMC on the Ni substrate is Ni_3In_7 .

As shown in Fig. 8, the residual In-rich phase and Cu particles in the *in situ* reaction zone are decreased gradually with increasing bonding time, and the thickness of the Cu@IMC is increased. The thickness of $\text{Cu}_{11}\text{In}_9$ and Ni_3In_7 interfacial IMC

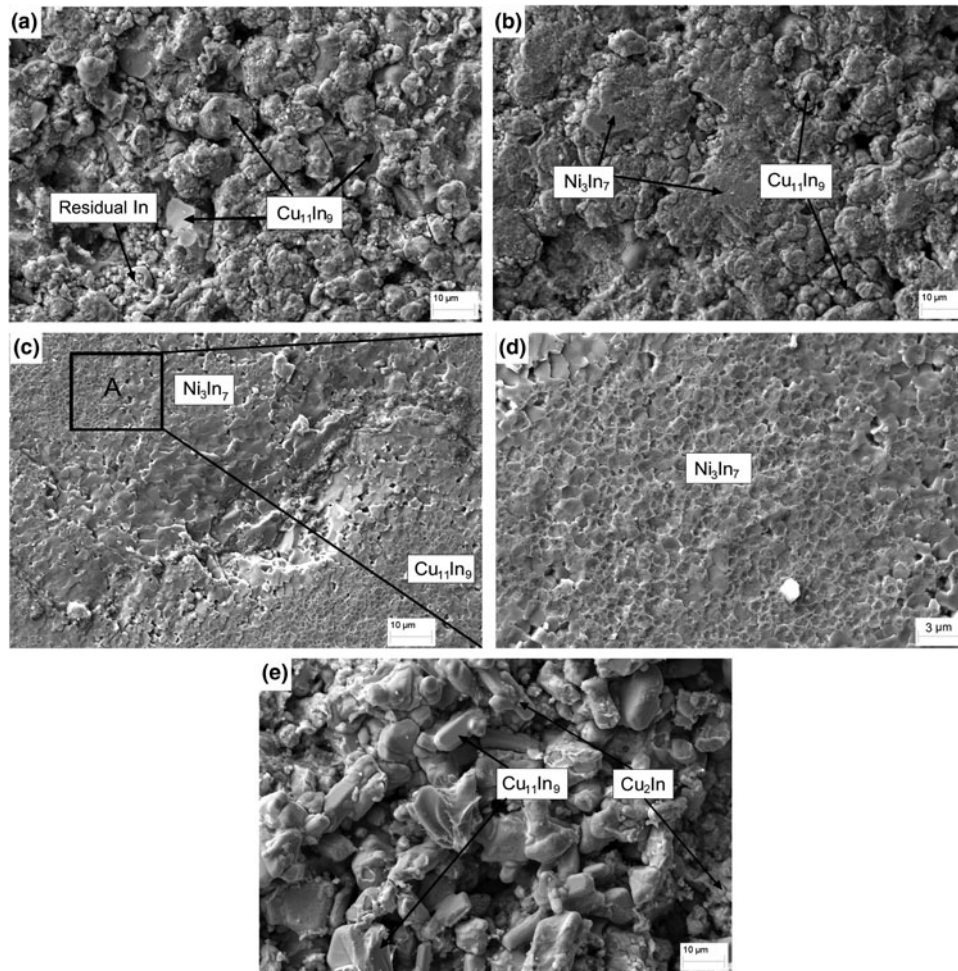


Figure 6: Fracture morphologies of Cu/In–45Cu/Ni solder joints at different bonding times: (a) 15 min, (b) 30 min, (c and d) 60 min, and (e) 120 min.

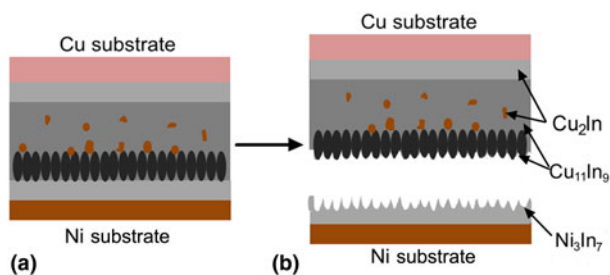


Figure 7: Shear fracture process of the Cu/In–45Cu/Ni solder joint at 60 min: (a) before shearing and (b) after shearing.

layer is both increased with increasing bonding time, and the interfacial IMCs layers are connected with the IMCs of the *in situ* reaction zone when bonding time is increased to 20 min.

As shown in Figs. 8(a) and 8(b), the thin $\text{Cu}_{11}\text{In}_9$ IMC is formed on the Cu particles surface at 0.5 min, which indicates that the nucleation and growth of $\text{Cu}_{11}\text{In}_9$ phase are very rapid during bonding. The bonding process is slow when In solder is

used for bonding because the IMCs in the solder joint are only obtained by the reaction of In atoms and diffused Cu and Ni atoms from substrates. However, the In atoms can react quickly with the uniformly distributed Cu particles in the *in situ* reaction zone of solder joints using In–45Cu solder for bonding. In addition, the specific surface area of Cu atoms in the liquid In is increased after adding Cu particles, and the reaction between In and Cu atoms is promoted greatly. Therefore, the Cu@IMC is obtained quickly after bonding for 0.5 min.

Once the $\text{Cu}_{11}\text{In}_9$ phase is encapsulated, the subsequent growth of $\text{Cu}_{11}\text{In}_9$ depends mainly on the solid diffusion of Cu and In atoms, and then, the process is relatively slow. In and Cu atoms both follow the downhill diffusion mechanism, and the atomic diffusion channel at 20 min is longer than that at 0.5 min due to the increased IMCs thickness. The diffusion rate of In atoms at 20 min can be regarded as identical to that at 0.5 min, and thus, the reaction process of In and Cu atoms at 20 min is retarded for the lengthened diffusion channel. Therefore, the growth rate of IMCs thickness is decreased with the increasing IMCs thickness.

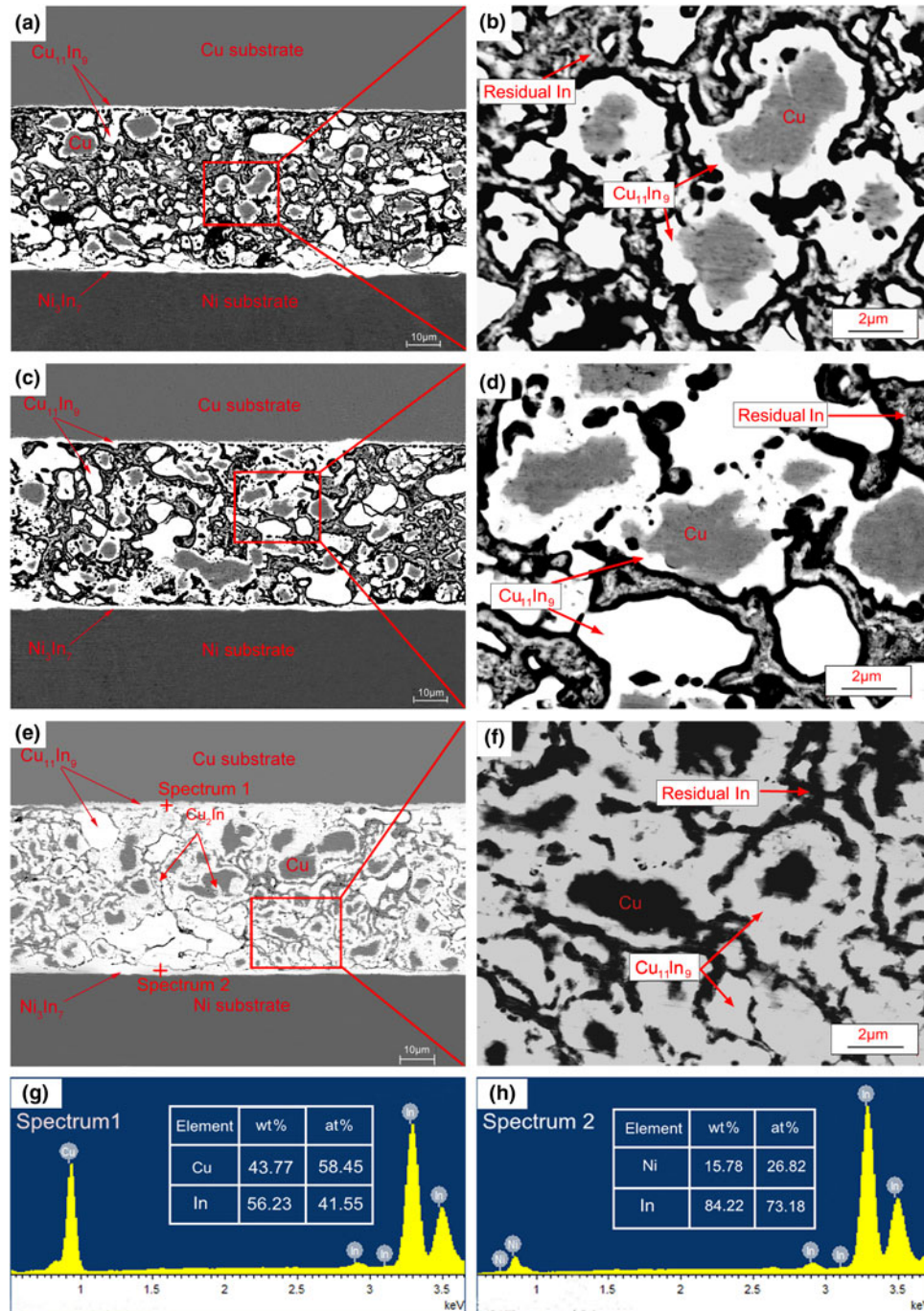


Figure 8: Microstructure of Cu/In-45Cu/Ni solder joints at different bonding times: (a and b) 0.5 min, (c and d) 5 min, (e and f) 20 min, (g) spectrum 1, and (h) spectrum 2.

In the *in situ* reaction zone, the IMCs nucleate and grow on the interface of Cu particles and liquid In phase. The excess In phase is gradually consumed with the increasing bonding time, and In-Cu IMCs and residual Cu particles are obtained finally after the bonding time of 20 min in the solder joint [Fig. 8(e)]. As shown in Fig. 8(e), a thin new phase appears between $\text{Cu}_{11}\text{In}_9$ phase and Cu particles, and EDS results show that it is Cu_2In . $\text{Cu}_{11}\text{In}_9$ phase is continuously converted to Cu_2In

phase by reacting with diffused Cu atoms, and Cu_2In phase continues to grow along the $\text{Cu}_{11}\text{In}_9$ /Cu interface with increasing bonding time [42].

Meanwhile, the island-shaped IMCs phase is found beside the Cu particles in the solder joint at 20 min. It may be formed by the reaction of the small Cu particles with In, and it may shed from the IMCs on the Cu particles surface. The amount of the IMCs in the *in situ* reaction zone is increased with

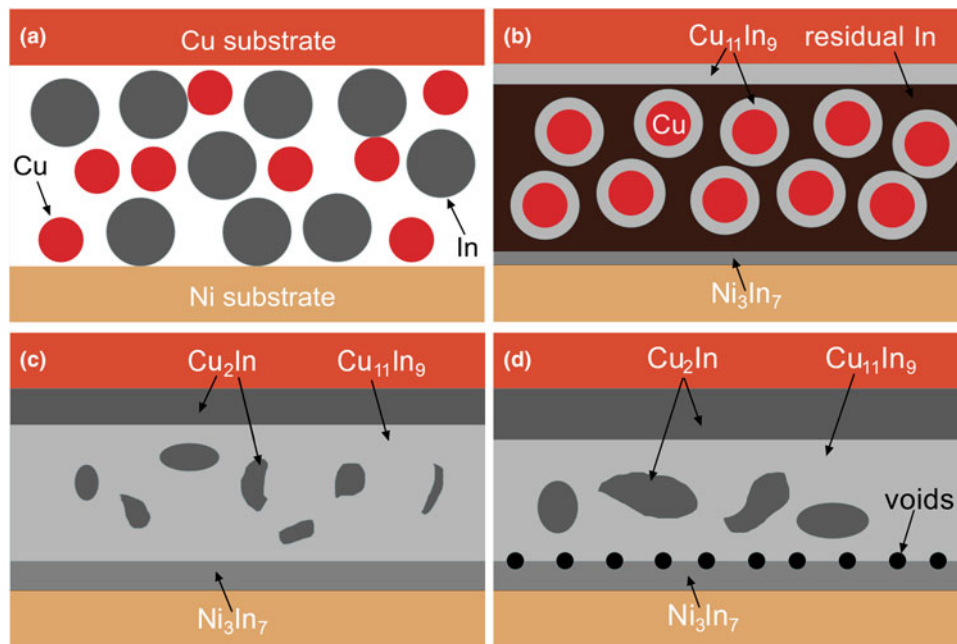


Figure 9: The schematic drawing of the microstructure evolution of Cu/In–45Cu/Ni solder joints at 260 °C for different times: (a) before bonding, (b) 0.5–20 min, (c) 60 min, and (d) 120 min.

increasing bonding time, to a certain extent, the IMCs contact with each other and combine with the growing IMCs on the substrates, and thus, the interconnection between Ni and Cu substrates is realized [as shown in Fig. 8(e)].

According to the Cu–In and Ni–In phases transformation of solder joints at different bonding times in Figs. 1 and 8, the schematic drawing of the microstructure evolution of Cu/In–45Cu/Ni solder joints formed at 260 °C is obtained (Fig. 9).

Conclusions

In this study, Cu and Ni substrates were bonded by using In–45Cu composite solder paste. The microstructure and the mechanical property of Cu/In–45Cu/Ni solder joints were investigated under reflowed at 260 °C for 15–120 min. In addition, the IMCs growth mechanism was obtained after discussing the microstructure evolution between 0.5 and 120 min. According to the experimental results, the conclusions are summarized as follows:

(1) The IMCs volume ratio of Cu/In–45Cu/Ni solder joints is increased firstly and then decreased with increasing bonding time of 15–120 min, and the maximum IMCs volume ratio of the solder joint is 95.8% at 60 min. The interfacial IMCs Cu/In–45Cu/Ni solder joints with dense microstructure at 60 min are Cu_2In and Ni_3In_7 phases, respectively, and the *in situ* reaction zone is composed of a large amount of $\text{Cu}_{11}\text{In}_9$ phase and a small amount of Cu_2In phase.

- (2) The shear strength of Cu/In–45Cu/Ni solder joints is increased firstly and then decreased with increasing bonding time, and the maximum value of 15.21 MPa is obtained at 60 min. The shear fracture mode is brittle intergranular fracture.
- (3) The *in situ* reaction zone consists of unreacted In phase, Cu particles, and Cu@IMC in the solder joints at 0.5–20 min. The thickness of the interfacial IMCs and the Cu@IMC are both increased continuously with increasing bonding time, which ultimately realizes the interconnection of Cu–Ni substrates.

Experimental

The In solder powder with a diameter of about 4–10 μm was used as the matrix, and about 45 wt% micron-sized Cu particles with a purity of 99.9% and a diameter of about 2–6 μm were added into In solder powder. In–45Cu composite solder powder was obtained after mixing In solder and Cu particles, and the morphology of In–45Cu powder was shown in Fig. 10(a). The Cu and In particles were evenly distributed in In–45Cu powder, and the size distribution of In and Cu particles was shown in Fig. 10(b). Then, about 11 wt% rosin flux was added in In–45Cu solder powder, and In–45Cu solder paste was obtained after long-time mechanical blending.

The size of the Cu substrate was 12 mm \times 12 mm \times 4 mm, and that of the Ni substrate was 10 mm \times 10 mm \times 4 mm. In–45Cu solder paste was evenly coated between Cu and Ni substrates, and the Cu/In–45Cu/Ni sandwich structure sample

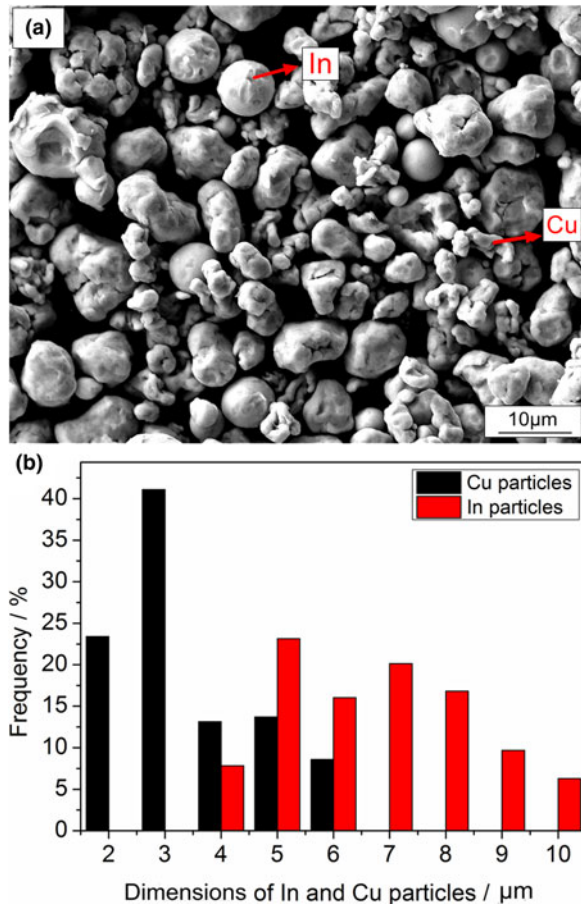


Figure 10: (a) Morphology of In-45Cu solder powder and (b) distribution of In and Cu particles dimensions.

was obtained. The sample preparation process and the experimental platform were shown in Supplementary Figure. The Cu/In-45Cu/Ni sample was placed in the TWB-100 wafer bonding machine under a vacuum of 1–5 Pa with a bonding temperature of 260 °C, a bonding pressure of 5 MPa, and a bonding time of 0.5–120 min. The Cu/In-45Cu/Ni solder joints were air-cooled to room temperature and washed by alcohol after bonding. The microstructure of the Cu/In-45Cu/Ni solder joint was observed by Zeiss supra 55 scanning electron microscope (SEM) equipped with EDS, and the phase composition of IMCs was analyzed by EDS. The IMCs volume ratio of the solder joints was measured by the ImageJ software.

The shear strength of the Cu/In-45Cu/Ni solder joint was tested by the UTMS 5305 metal material universal testing machine with a stretching rate of 0.02 mm/s. The average values of all data were taken after being tested for three times. The shear fractures of Cu/In-45Cu/Ni solder joints were observed by SEM.

Acknowledgment

This research was financially supported by the National Natural Science Foundation of China (Grant No. 51865006).

Supplementary material

To view supplementary material for this article, please visit <https://doi.org/10.1557/jmr.2020.194>.

References

1. F. Roccaforte, F. Giannazzo, F. Iucolano, J. Eriksson, M.H. Weng, and V. Raineri: Surface and interface issues in wide band gap semiconductor electronics. *Appl. Surf. Sci.* **256**, 5727–5735 (2010).
2. D. Wang, D. Li, M. Zhao, Y. Xu, and Q.F. Wei: Multifunctional wearable smart device based on conductive reduced graphene oxide/polyester fabric. *Appl. Surf. Sci.* **454**, 218–226 (2018).
3. F. Roccaforte, P. Fiorenza, G. Greco, R.L. Nigro, F. Giannazzo, F. Iucolano, and M. Saggio: Emerging trends in wide band gap semiconductors (SiC and GaN) technology for power devices. *Microelectron. Eng.* **187**, 66–77 (2017).
4. L.M. Yin, S. Wei, Z.L. Xu, and Y.F. Geng: The effect of joint size on the creep properties of microscale lead-free solder joints at elevated temperatures. *J. Mater. Sci.: Mater. Electron* **24**, 1369–1374 (2013).
5. S. Stoyanov, C. Bailey, and M. Desmulliez: Optimisation modelling for thermal fatigue reliability of lead-free interconnects in fine-pitch flip-chip packaging. *Solder. Surf. Mt. Technol.* **21**, 11–24 (2009).
6. E.H. Amalu, N.N. Ekere, R.S. Bhatti, S. Mallik, G. Takyi, and A.O.A. Ibhado: Numerical investigation of thermo-mechanical behaviour of ball grid array solder joint at high temperature excursion. *Adv. Mater. Res.* **367**, 287–292 (2011).
7. H.Y. Zhao, J.H. Liu, Z.L. Li, Y.X. Zhao, H.W. Niu, X.G. Song, and H.J. Dong: Non-interfacial growth of Cu₃Sn in Cu/Sn/Cu joints during ultrasonic-assisted transient liquid phase soldering process. *Mater. Lett.* **186**, 283–288 (2017).
8. W. Chen and J. Duh: Suppression of Cu₃Sn layer and formation of multi-orientation IMCs during thermal aging in Cu/Sn-3.5Ag/Cu-15Zn transient liquid-phase bonding in novel 3D-IC Technologies. *Mater. Lett.* **186**, 279–282 (2017).
9. X.D. Liu, S.L. He, and H. Nishikawa: Thermally stable Cu₃Sn/Cu composite joint for high-temperature power device. *Scr. Mater.* **110**, 101–104 (2016).
10. R.H. Zhang, F. Guo, J.P. Liu, H. Shen, and F. Tai: Morphology and growth of intermetallics at the interface of Sn-based solders and Cu with different surface finishes. *J. Electron. Mater.* **38**, 241–251 (2009).
11. F.C. Tai, K.J. Wang, and J.D. Duh: Application of electroless Ni-Zn-P film for under-bump metallization on solder joint. *Scr. Mater.* **61**, 748–751 (2009).
12. T. Kadoguchi, N. Take, K. Yamanaka, S. Nagao, and K. Suganuma: Highly thermostable joint of a Cu/Ni-P plating/

- Sn–0.7Cu solder added with Cu balls. *J. Mater. Sci.* **52**, 3244–3254 (2017).
13. **H.J. Dong, Z.L. Li, X.G. Song, H.Y. Zhao, H. Tian, J.H. Liu, and J.C. Yan:** Grain morphology evolution and mechanical strength change of intermetallic joints formed in Ni/Sn/Cu system with variety of transient liquid phase soldering temperatures. *Mater. Sci. Eng. A* **705**, 1026–1031 (2017).
 14. **L.P. Mo, C.W. Guo, Z. Zhou, F.S. Wu, and C.Q. Liu:** Microstructural evolution of Cu–Sn–Ni compounds in full intermetallic micro-joint and *in situ* micro-bending test. *J. Mater. Sci.: Mater. Electron* **29**, 11920–11929 (2018).
 15. **Y. Zhong, M. Huang, H. Ma, W. Dong, Y.P. Wang, and N. Zhao:** *In situ* study on Cu–Ni cross-interaction in Cu/Sn/Ni solder joints under temperature gradient. *J. Mater. Res.* **31**, 609–617 (2016).
 16. **H.J. Ji, Y.F. Qiao, and M.Y. Li:** Rapid formation of intermetallic joints through ultrasonic-assisted die bonding with Sn–0.7Cu solder for high temperature packaging application. *Scr. Mater.* **110**, 19–23 (2016).
 17. **Y.S. Huang, H.Y. Hsiao, C. Chen, and K.N. Tu:** The effect of a concentration gradient on interfacial reactions in microbumps of Ni/SnAg/Cu during liquid-state soldering. *Scr. Mater.* **66**, 741–744 (2012).
 18. **N. Zhao, M.Y. Wang, Y. Zhong, H.T. Ma, Y.P. Wang, and C.P. Wong:** Effect of Zn content on Cu–Ni cross-interaction in Cu/Sn–xZn/Ni micro solder joints. *J. Mater. Sci.: Mater. Electron* **29**, 5064–5073 (2018).
 19. **J.W. Yoon and B.S. Lee:** Sequential interfacial reactions of Au/In/Au transient liquid phase-bonded joints for power electronics applications. *Thin Solid Films* **660**, 618–624 (2018).
 20. **Y.H. Tian, C.J. Hang, X. Zhao, B.L. Liu, N. Wang, and C.Q. Wang:** Phase transformation and fracture behavior of Cu/In/Cu joints formed by solid–liquid interdiffusion bonding. *J. Mater. Sci.: Mater. Electron* **25**, 4170–4178 (2014).
 21. **S.K. Lin, Y.H. Wang, and H.C. Kuo:** Strong coupling effects during Cu/In/Ni interfacial reactions at 280 °C. *Intermetallics* **58**, 91–97 (2015).
 22. **T.T. Dorini and L.T.F. Eleno:** Thermodynamic reassessment of the Ni–In system using ab-initio data for end-member compound energies. *Calphad* **62**, 42–48 (2018).
 23. **L. Noren, R.L. Withers, and Y. Tabira:** New B8–B8 phases in the Ni–In system. *J. Alloys Compd* **309**, 179–187 (2000).
 24. **P.J. Shang, Z.Q. Liu, D.X. Li, and J.K. Shang:** Intermetallic compound identification and Kirkendall void formation in eutectic SnIn/Cu solder joint during solid-state aging. *Philos. Mag. Lett.* **91**, 410–417 (2011).
 25. **V.A. Baheti, S. Kashyap, K. Praveen, K. Chattopadhyay, and A. Paul:** Bifurcation of the Kirkendall marker plane and the role of Ni and other impurities on the growth of Kirkendall voids in the Cu–Sn system. *Acta Mater.* **131**, 260–270 (2017).
 26. **C. Yu, Y. Yang, Y.K. Wang, J.J. Xu, J.M. Chen, and H. Lu:** Relation between Kirkendall voids and intermetallic compound layers in the SnAg/Cu solder joints. *J. Mater. Sci.: Mater. Electron* **23**, 124–129 (2012).
 27. **H. Liu, K. Wang, K.E. Aasmundtveit, and N. Hoivik:** Intermetallic compound formation mechanisms for Cu–Sn solid–liquid interdiffusion bonding. *J. Electron. Mater.* **41**, 2453–2462 (2012).
 28. **K. Chu, Y. Sohn, and C. Moon:** A comparative study of Cu/Sn/Cu and Ni/Sn/Ni solder joints for low temperature stable transient liquid phase bonding. *Scr. Mater.* **109**, 113–117 (2015).
 29. **L.D. Chen, M.L. Huang, and S.M. Zhou:** Effect of electromigration on intermetallic compound formation in line-type Cu/Sn/Cu and Cu/Sn/Ni interconnects. In *60th Electronic Components and Technology Conference (ECTC)* (IEEE: Las Vegas, NV, USA, 2010).
 30. **M.J. Rizvi, Y.C. Chan, C. Bailey, H. Lu, M.N. Islam, and B.Y. Wu:** Wetting and reaction of Sn–2.8Ag–0.5Cu–1.0Bi solder with Cu and Ni substrates. *J. Electron. Mater.* **34**, 1115–1122 (2005).
 31. **S.Y. Piao and S. Lidin:** A new compound in the Cu–In system—the synthesis and structure of Cu₁₀In₇. *Z. Anorg. Allg. Chem.* **634**, 2589–2593 (2008).
 32. **L. Sun, M.H. Chen, and L. Zhang:** Microstructure evolution and grain orientation of IMC in Cu–Sn TLP bonding solder joints. *J. Alloys Compd.* **786**, 677–687 (2019).
 33. **H. Pao, J.Y. Huang, H.J. Ji, and M.Y. Li:** Enhancing the solid/liquid interfacial metallurgical reaction of Sn + Cu composite solder by ultrasonic-assisted chip attachment. *J. Alloys Compd.* **784**, 603–610 (2019).
 34. **J.B. Lee, H.Y. Hwang, and M.W. Rhee:** Reliability investigation of Cu/In TLP bonding. *J. Electron. Mater.* **44**, 435–441 (2015).
 35. **H.L. Li, A. Rong, C.Q. Wang, and Z. Jiang:** In situ quantitative study of microstructural evolution at the interface of Sn_{3.0}Ag_{0.5}Cu/Cu solder joint during solid state aging. *J. Alloys Compd.* **634**, 94–98 (2015).
 36. **A.A. El-Daly, A. Fawzy, S.F. Mansour, and M.J. Younis:** Thermal analysis and mechanical properties of Sn–1.0Ag–0.5Cu solder alloy after modification with SiC nano-sized particles. *J. Mater. Sci.: Mater. Electron* **24**, 2976–2988 (2013).
 37. **F.S. Wu, B. Wang, B. Du, B. An, and Y.P. Wu:** Effect of stand-off height on microstructure and tensile strength of the Cu/Sn₉Zn/Cu solder joint. *J. Electron. Mater.* **38**, 860–865 (2009).
 38. **C.M. Liu, D.J. Yu, and X. Chen:** Simulation implementation on the direction prediction of crack propagation based on the first principal stress. *Key Eng. Mater.* **795**, 361–366 (2019).
 39. **T.R. Bieler, P. Eisenlohr, F. Roters, D. Kumar, D.E. Mason, M.A. Crimp, and D. Raabe:** The role of heterogeneous

- deformation on damage nucleation at grain boundaries in single phase metals. *Int. J. Plast.* **25**, 1655–1683 (2009).
40. **D.Y. Lee, E.V. Barrera, J.P. Stark, and H.L. Marcus:** The influence of alloying elements on impurity induced grain boundary embrittlement. *Metall. Mater. Trans. A* **15**, 1415–1430 (1984).
41. **C.L. Briant:** On the chemistry of grain boundary segregation and grain boundary fracture. *Metall. Mater. Trans. A* **21**, 2339–2354 (1990).
42. **F.F. Tian, Z.Q. Liu, and J.D. Guo:** Phase transformation between $\text{Cu}(\text{In},\text{Sn})_2$ and $\text{Cu}_2(\text{In},\text{Sn})$ compounds formed on single crystalline Cu substrate during solid state aging. *J. Appl. Phys.* **115**, 1335 (2014).